China Ocean Eng., Vol. 29, No. 4, pp. 473 – 488

DOI 10.1007/s13344-015-0033-z, ISSN 0890-5487

Simulation of Storm Surge and Wave Due to Typhoon Isewan (5915)*

Jin-Hee YUK[a], Kyeong Ok KIM[b], Han Soo LEE[c] and Byung Ho CHOI[d, 1]

[a] *Disaster Management HPC Technology Research Center*, *Korea Institute of Science and Technology Information*, *Yuseong*, *Daejeon 305-806*, *Korea*

[b] *Marine Radionuclide Research Center*, *Korea Institute of Ocean Science & Technology*, *Ansan 426-744*, *Korea*

[c] *Graduate School of Science and Engineering*, *Saitama University*, *Saitama 338-8570*, *Japan*

[d] *Department of Civil and Environmental Engineering*, *Sungkyunkwan University*, *Suwon 440-746*, *Korea*

(Received 17 February 2014; received revised form 1 September 2014; accepted 28 October 2014)

ABSTRACT

An integrally coupled wave-tide-surge model was developed and then applied to the simulation of the wave-typhoon surge for the typhoon Isewan (typhoon Vera (5915)), which is the strongest typhoon that has struck Japan and caused incalculable damage. An integrally coupled tide-surge-wave model using identical and homogeneous meshes in an unstructured grid system was used to correctly resolve the physics of wave-circulation interaction in both models. All model components were validated independently. The storm surge and wave properties such as the surge height, the significant wave height, wave period and direction were reproduced reasonably under the meteorological forcing, which was reprocessed to be close to the observations. The resulting modeling system can be used extensively for the prediction of the storm surge and waves and the usual barotropic forecast.

Key words: *typhoon Isewan*; *storm surge*; *wave*; *tide*; *coupled wave-tide-surge model*

1. Introduction

Typhoon Vera (5915) is the strongest typhoon that has struck Japan, causing incalculable damage to the country. Typhoon Vera hit central Japan including Nagoya City, which is the largest city in the central region, and resulted in record damage to the region due to high tides and floods. The typhoon led to casualties and the number of missing persons totaled approximately 5000, with an additional 39000 people injured (JWF, 2005). The JMA (Japan Meteorological Agency) gives a new name to typhoons that are very destructive and result in significant damages. Therefore, the name typhoon Isewan is given to typhoon Vera (5915), in which, "wan" means "a bay" in Japanese.

Owing to the above reasons, many studies have been carried out in order to reproduce the typhoon Isewan based on wave, tide and surge models, with an ultimate goal of preventing future coastal disasters. Shibaki *et al*. (1998) developed the integrated numerical research system for the prevention and estimation of coastal disasters (INSPECT) and applied it to the simulation of typhoon Isewan. This system estimates wave, tide and storm surge, but requires eight sub-domains of the model to perform

* This study was supported by the China-Korea Cooperative Research Project funded by CKJORC as well as a major project titled the development of the marine environmental impact prediction system funded by KIOST, and supported by the project of KISTI for the development of HPC-based management system against national-scale disaster.

1 Corresponding author. E-mail: bhchoi.skku@gmail.com

the calculation of the tide-surge for the large model domain, which includes the Pacific Ocean. These eight sub-domains are also needed to correctly calculate the tide in the shallow water of the bay against the calculation of the tide for the ocean based on a coarse mesh. In a different study, Shibaki (2004) used twelve sub-domains for the same tide-surge simulation from above. Kawasaki *et al*. (2010) developed the storm surge and high wave-induced inundation model based on the Myers-based typhoon model, a depth-averaged flow model with a one-way nesting method, the wave model SWAN and an inundation flow model using the CIP (Constrained Interpolation Profile) method. Kobayashi (2002) estimated the wave data for the typhoon Isewan using a wind wave model (SWAN) and discussed the model's application for the prevention of coastal disasters and the protection of the marine environment. The TTRI (Transportation Technical Research Institute, 1959) also estimated wave characteristics using their graphical calculation method and reported that this method could account for the characteristics of waves in moving fetches in shallow water. Yamaguchi *et al*. (2012) carried out shallow water wave hindcasting for each of 14 selected typhoons from 1921 to 1972, including the typhoon Isewan in the Ise Bay. They also used a nested grid in the simulation with the mesh sizes of 5 km in the northwest Pacific Ocean and 0.1 km in the Ise Bay. Yamaguchi *et al*. (2010, 2013a, 2013b) showed figure collections for the spatial distribution of the lowest sea level pressure induced by strong typhoons from 1921 to 1972 in the Ise Bay and wind distributions including the typhoon Isewan in order to create correct meteorological forcing for the storm surge simulation in the bays.

Meanwhile, some studies use wave and tide-surge models separately, or loosely couple them by using one unstructured circulation mesh and several structured wave meshes by passing information via external files (Dietrich *et al*., 2011). In addition, several of the models used require sub-domains or nesting to calculate the storm surge or wave properties of the typhoon. However, these approaches are insufficient, and therefore, an integrally (fully) coupling model of wave-tide-surge based on identical and homogeneous unstructured mesh has been developed.

According to Dietrich *et al*. (2011), waves and circulation should be coupled because they can intersect. Water levels and currents affect the propagation of waves and the location of wave-breaking zones. Wave transformation produces the radiation stress gradients that force set-up and currents. Wind-driven waves influence the vertical momentum mixing and bottom friction, which in turn influence the circulation. The percentages of wave-induced setup are 5−20 in regions across a broad continental shelf and up to 35 in regions with a steep slope (Dietrich *et al*., 2011). Choi *et al*. (2013) showed that the surge elevation and current were significantly changed by the wave radiation stress in shallow water areas. Additionally, the surge elevation reproduced by the integrally coupled model, which is the same as that in this study, agreed well with the observations, while the results computed by the un-coupled model tended to be underestimated.

Generally, models with structured meshes employ nesting or overlapping, which may cause errors in the interpolation procedure (Zijlema, 2010). Hence, this study is based on an unstructured mesh, which does not require nesting or overlapping of structured wave meshes and interpolation. The problem of wave reflection in the nesting boundary due to incomplete feedback from the mother's domain was not a necessary consideration. The waves and storm surge were allowed to develop along the continental shelf and interact with the complex near-shore environment. The coupled system

consists of unstructured-mesh SWAN waves and ADCIRC based on the same unstructured mesh. This identical and homogeneous mesh allows for the physics of wave-circulation interactions to be correctly resolved in both models. The hydrodynamic model (ADCIRC) is driven partly by the radiation stress gradients that are computed by using information from the spectral wind wave model (SWAN), which uses the water levels and currents computed in the hydrodynamic model.

As described above, many studies have focused on typhoon Isewan, which had significantly destructive power, in order to study the prevention of coastal disasters. We also selected this typhoon for the same reason, despite the fact that it is an older natural disaster. We also selected this typhoon for the simulation of waves and storm surge because even though typhoon Isewan happened over half a century ago, there are several observations and documents that prove to be helpful for this study. In addition, among the several papers that developed simulation models of typhoon Isewan, the approach taken in this study, based not only on the fully coupled model of wave-tide-surge but also on unstructured meshes, has never been tried before. The modeling system introduced in this study and its strengths are described in detail in the next section and also explained previously. The integrally coupled wave-tide-surge model introduced in this study has also been used for the simulations of other typhoons and can reproduce the storm surge and wave properties reasonably (Choi *et al*., 2013; Kim *et al*., 2013a, 2013b). Hence, reproduction of this coupled model was demonstrated in previous studies. In this study, we focus on one significant typhoon and analyze its waves and storm surge from various fields using several observations and research. It is a significant achievement to be able to reproduce a critical issue using the appropriate prediction tool, as it is completed in this study. The modeling methods and results are presented and discussed in terms of the application of the modeling system for hindcasting and forecasting of the tide-surge-wave.

2. Numerical Method

2.1 Wave Model

SWAN (Simulating WAves Nearshore) predicts the evolution in geographical space and time of the wave action density spectrum, with relative frequency (σ) and wave direction (θ), as governed by the action balance equation (Booij *et al*., 1999):

$$\frac{\partial N}{\partial t}+\nabla_x\left[\left(\boldsymbol{c}_{\mathrm{g}}+\boldsymbol{U}\right)N\right]+\frac{\partial c_\theta N}{\partial\theta}+\frac{\partial c_\sigma N}{\partial\sigma}=\frac{S_{\mathrm{tot}}}{\sigma}. \tag{1}$$

The terms on the left-hand side represent, respectively, the change in wave action in time *t*, the propagation of wave action in space (with ∇_x the gradient operator in geographic space, $\boldsymbol{c}_{\mathrm{g}}$, wave group velocity and $\boldsymbol{U}$, the ambient current vector), depth and current induced refraction and approximate diffraction (with propagation velocity or turning rate c_θ), and the shifting of wave action due to variations in the mean current and depth (with propagation velocity or shifting rate c_σ). The source term, S_{tot}, represents wave growth by wind, action lost due to whitecapping, surf breaking and bottom friction, and action exchanged between spectral components in deep and shallow water due to nonlinear effects. The associated SWAN parameterizations are given by Booij *et al*. (1999), with all

subsequent modifications as presented in version 40.72, including phase-decoupled refraction−diffraction (Holthuijsen *et al*., 2003), although diffraction is not enabled for the present simulations. The unstructured-mesh version of SWAN, named UnSWAN (Unstructured-mesh SWAN), implements an analog to the four-direction Gauss−Seidel iteration technique employed in the structured version, and it maintains SWAN's unconditional stability (Zijlema, 2010). SWAN computes the wave action density spectrum at the vertices of an unstructured triangular mesh, and it orders the mesh vertices so that it can sweep through them and update the action density using information from neighboring vertices.

2.2 Tide-Surge Model

ADCIRC (ADvanced CIRCulation model) is a continuous-Galerkin, finite-element, shallow-water model that solves for water levels and currents at a range of scales (Westerink *et al*., 2008; Luettich and Westerink, 2004; Atkinson *et al*., 2004; Dawson *et al*., 2006). The details of this solution have been published widely (http://www.nd.edu/~adcirc/manual.htm to see Users Manual and Theory Report) and will not be stated here.

2.3 Simulation Procedures

SWAN was used for wave computations and ADCIRC was used for tide and surge simulations, and a schematic of the communication between the two models is shown in Fig. 1. The basic structure of this coupling system was developed by Dietrich *et al*. (2010).

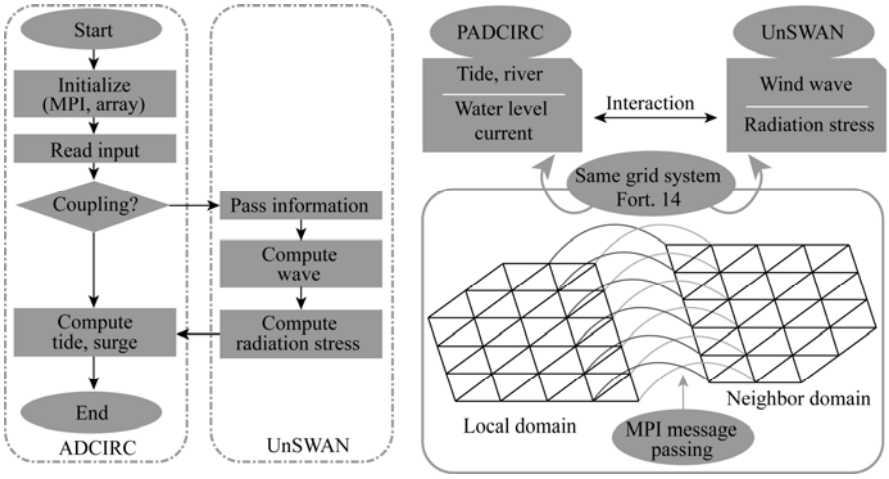

Fig. 1. Schematic of parallel communication between models and cores. Solid lines indicate communication for the edge-layer-based nodes between sub-meshes (intra-model and inter-core) (Choi *et al*., 2013).

SWAN is driven by wind speeds, water levels and currents computed at the vertices by ADCIRC. ADCIRC can accept marine winds in various formats, which are adjusted directionally to account for surface roughness (Bunya *et al*., 2010). Wind is calculated at the vertices through interpolating spatially and temporally with ADCIRC, and then, the results are passed to SWAN. Similarly, the water levels and ambient currents are computed in ADCIRC before being sent to SWAN, where they are used to re-compute the water depth and all relevant wave processes (wave propagation, depth-induced breaking, etc.).

The ADCIRC model is driven partially by the radiation stress gradients computed by using information from SWAN. These gradients, τ_s are computed by:

$$\tau_{sx,wave} = -\frac{\partial S_{xx}}{\partial x} - \frac{\partial S_{xy}}{\partial y}; \tag{2}$$

$$\tau_{sy,wave} = -\frac{\partial S_{xy}}{\partial x} - \frac{\partial S_{yy}}{\partial y}, \tag{3}$$

where, S_{xx}, S_{xy} and S_{yy} are the wave radiation stresses (Longuet–Higgins and Stewart, 1964; Battjes, 1972).

ADCIRC and SWAN run in series on the same local mesh and core. These two models "leap frog" through time, and each model is forced by information from the other model (Dietrich *et al*., 2011). SWAN employs a sweeping method to update the wave information at the computational vertices. Therefore, SWAN can take much larger time steps than ADCIRC, which has diffusion- and Courant-timestep limitations due to its semi-explicit formulation and its wetting and drying algorithm. Consequently, the coupling interval is designed to be the same as the time step used for SWAN.

As for the coupling between ADCIRC and SWAN, it is assumed that the wave properties are influenced by circulation in the near-shore and the coastal floodplain; thus, ADCIRC runs first on the single coupling interval.

The coupling procedures between the two models are described as follows. Focus is placed on the single coupling interval, which is the same as the time step of SWAN mentioned above. At the beginning of a coupling interval, ADCIRC can obtain the radiation stress gradients computed by SWAN at times corresponding to the beginning and end of the previous interval. ADCIRC uses the information by extrapolating the gradients of the previous coupling interval at all time steps in the current coupling interval. When the ADCIRC run is completed, the SWAN run is performed for one time step. At this time, SWAN takes the information obtained from ADCIRC at the same time. As mentioned above, this information includes wind speeds, water levels and currents computed by ADCIRC at times corresponding to the beginning and end of the current coupling interval. These variables are averaged for the current one coupling interval, i.e., a single SWAN time step, and are used as the driving forces for SWAN at each time step.

To summarize the information shared and coupled from the two models in the above, ADCIRC uses the radiation stress gradients from SWAN, which is always extrapolated forward in time, whereas SWAN uses the wind speeds, water levels and currents from ADCIRC, which are always averaged to agree with a single SWAN time step.

3. Model Setup for Simulation of Typhoon Isewan

3.1 Meteorological Forcing Input

For the simulation, Grid Point Values (GPVs) of sea level pressure and air and sea surface temperature at 50 km intervals over the Northeast Asian seas were digitized by the Japan Weather Association (JWA). Those values were interpolated to a dense (1/12)° grid resolution at hourly

intervals from a six hourly dataset for the coupled model. The overall marine wind fields were computed by adopting the Planetary Marine Boundary Layer model (Cardone, 1969), and then, the typhoon model winds from the Rankin vortex model (Fujita, 1952) were inserted. Temporal interpolation along the typhoon track was also performed. The meteorological data obtained through the above two methods were not appropriate for the storm surge simulation, and thus, the data quality were improved by a blending method that used both datasets (Choi *et al*., 2013).

Fig. 2 shows the computed results of the pressure and wind vector fields for the typhoon Isewan at an interval of 6 hr from 06:00 UTC Sep. 26. The track of the typhoon Isewan selected for the simulation is shown in Fig. 3. Typhoon Isewan formed on Sep. 21 off the coast of Saipan and tracked northwestward with center pressures of 894 hPa at 06:00 UTC Sep. 23 and 900 hPa at 06:00 UTC Sep. 24. It then moved north and northeastward with a pressure of approximately 940 hPa passing near Nagoya City, Japan. The typhoon Isewan made landfall with peak gusts of 258 km/hr, while the strongest sustained wind speed was recorded in Nagoya City at over 161 km/hr. Sustained wind speeds of over 81 km/hr were recorded along the path of Japan from Kyushu to Hokkaido (JWF, 2005).

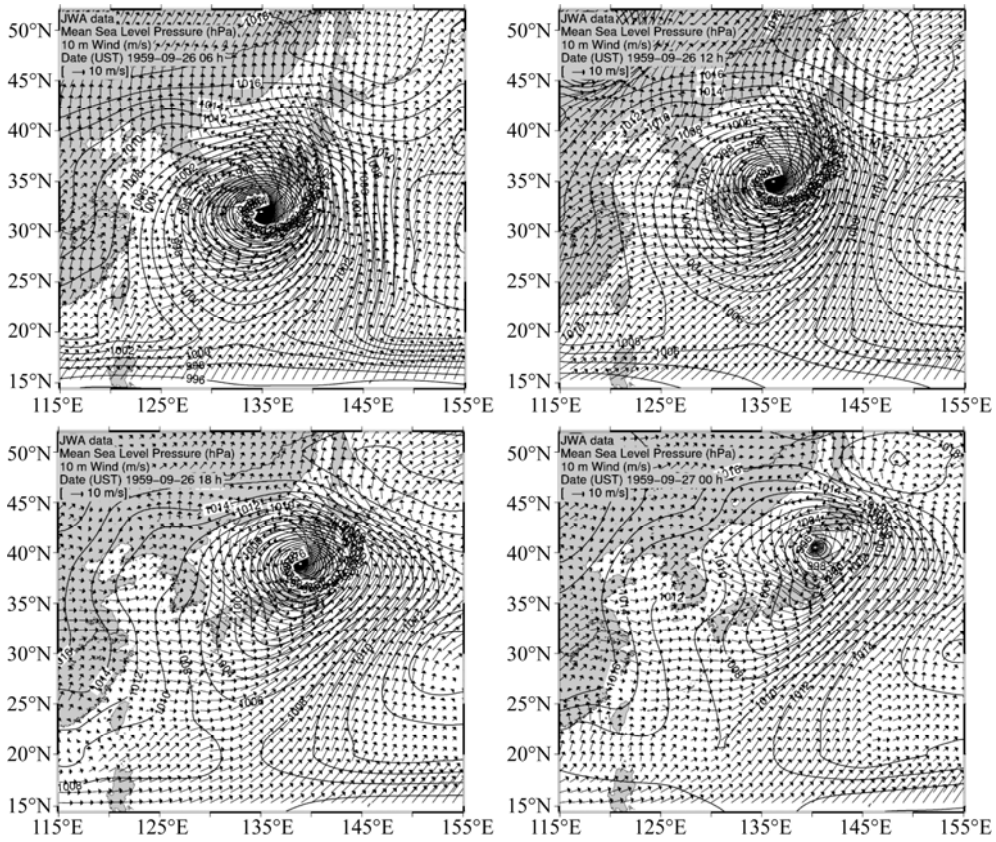

Fig. 2. Distribution of wind and air pressure fields for the typhoon Isewan (typhoon Vera (5915)).

3.2 Model Parameters

The model domain and complex mesh resolutions are shown in Fig. 4. The model domain is

extended to the Yellow Sea, the East China Sea and the western Pacific Ocean, including hundreds of islands. This mesh system has a local resolution down to 50 m. This is a sufficient resolution for the wave-transformation zones near the coasts and allows for intricate representation of various natural and man-made geographic features where the storm surge is collected and focused on. The mesh system contains 173507 vertices and 320193 triangular elements. The bathymetry data of model domain are composed by GEBCO (Jones, 2003) and the bathymetric and topographic data with a 50-m resolution of the Japanese Government (Central Disaster Management Council, 2003). An open boundary driving force was applied in the form of specifications based on NAO's (National Astronomical Observatory) tidal predictions (Matsumoto *et al*., 2000) along the model's open water boundary.

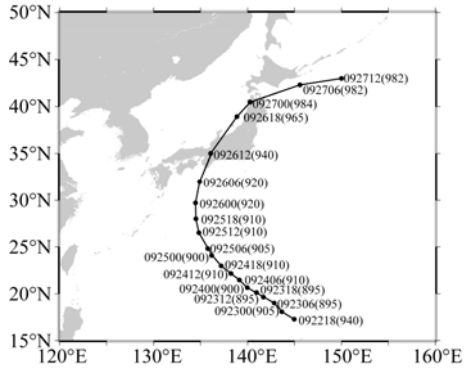

Fig. 3. Track of the typhoon Isewan. The numbers indicate date (MMDDhh (UST)). The numbers in the parenthesis indicate the typhoon center pressure (hPa).

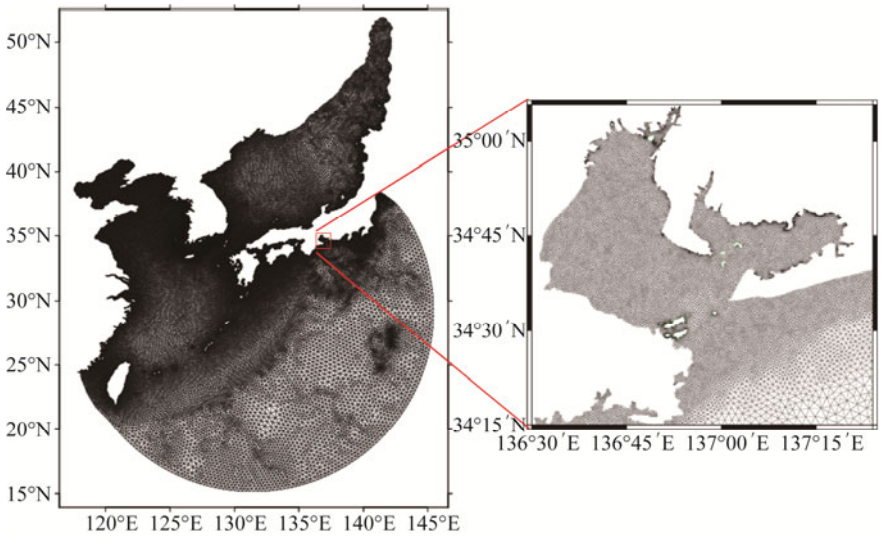

Fig. 4. Model domain, mesh system and location of the Ise Bay.

4. Simulation Results

The modeled data were compared with the observed data in terms of the meteorological driving force and its results at four weather and five water level observation stations (Fig. 5). The sources of observation data are the JMA report (1961), TTRI report (1959) and Shibaki's paper (2004).

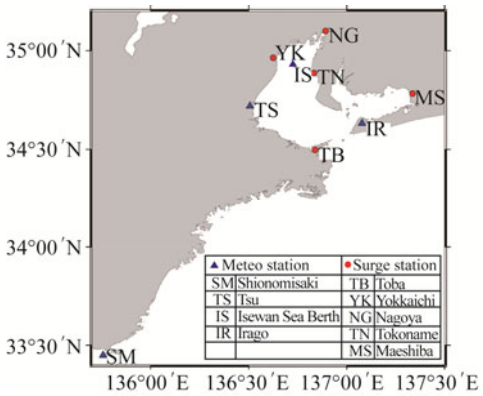

Fig. 5. Locations of observation stations marked with circles (water level) and triangles (meteorological data).

Fig. 6 shows the comparison of the observed and calculated air pressure at Shionomisaki and Irago Stations. Fig. 7 illustrates the comparison between the observed and calculated wind data at three weather stations. The estimated wind speeds at three stations are different from the observations, but their directions are generally close to those observed. The air pressure used in the model agrees well with the observations, but the modeled wind speeds are larger than the observations. The overestimation may be attributed to a failure to fully consider topographical effects (Shibaki, 2004).

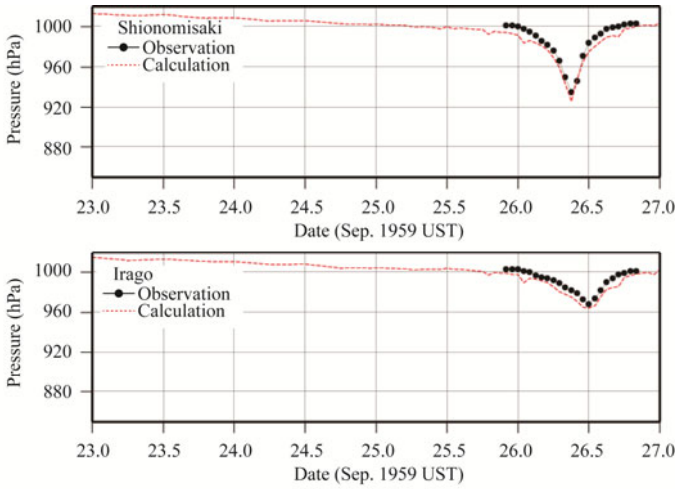

Fig. 6. Comparison of observed and calculated air pressure.

During the typhoon Isewan, it is reported that the largest surge height of 3.45 m was observed at Nagoya Port at 21:35 JST (12:35 UTC) Sep. 26, and our model results show 3.0 m at that station around that time (Fig. 8). The differences between the observed and simulated peaks of the surge heights are smaller than 0.5 m, except for the data from the Tokoname Station. In addition, except for the Toba Station, the time when the peak surge height occurs is reasonably predicted at four stations. The maximum positive surge heights in the Ise Bay were calculated realistically. Shibaki *et al*. (1998) showed that the higher the resolution of the mesh was, the better the simulation model was to reproduce the surge. The mesh resolution of this study is smaller than approximately 100 m inside the Ise Bay. Therefore, the

mesh condition also results in a reasonable surge height. The distribution of the maximum positive surge height is shown in Fig. 9. Fig. 10 shows the maximum negative surge height in the Ise Bay. The maximum negative surge height is larger along the west side of the Ise Bay, which is opposite in direction to the maximum positive surge height. In the Ise Bay, the southeasterly wind blew before the typhoon approached the bay (before approximately Sep. 26 12:00 UTC), while the wind direction changed to the southwest as soon as the typhoon passed through the bay (Fig. 7). In addition, there is an entrance to the Ise Bay in the south. The bay has a shallow water depth of smaller than 40 m from the northernmost reach of the bay to the entrance in the southernmost portion. That is, the southeasterly wind pushed the seawater into the northwest of the bay, and then, this seawater that entered the bay moved to the northeast of the bay due to the changed southwesterly wind. As a result, the maximum surge height was observed near the Nagoya Station. Owing to the above effects, the maximum positive surge height was also found in the Tsumi Bay, which is located at the east side of the Ise Bay.

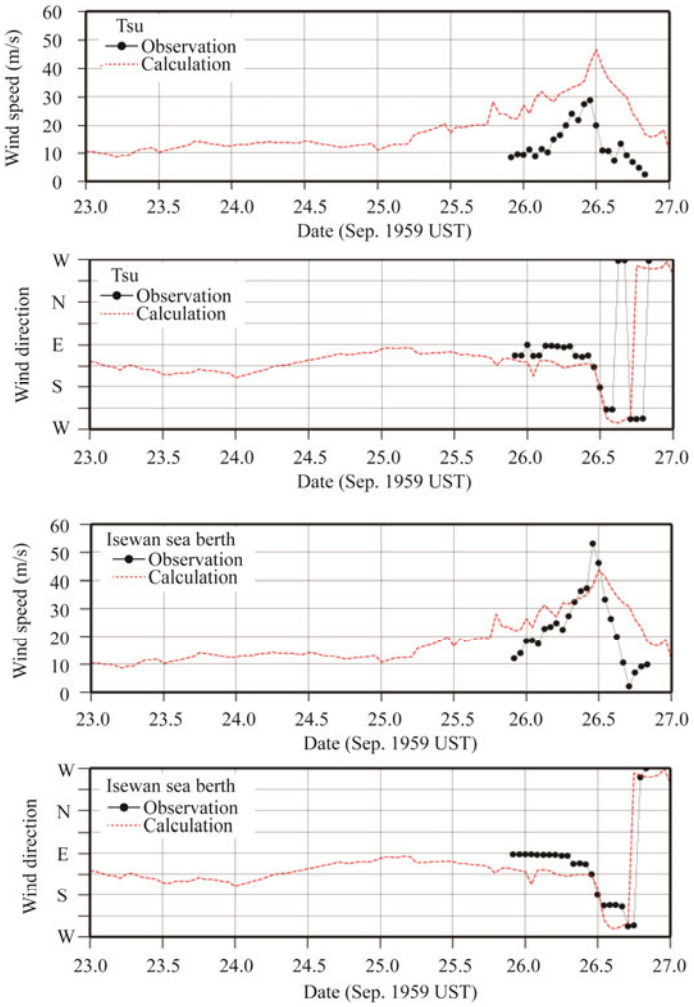

Fig. 7. Comparison of observed and calculated wind data at Tsu, Isewan-sea-berth and Irago Stations (to be continued)

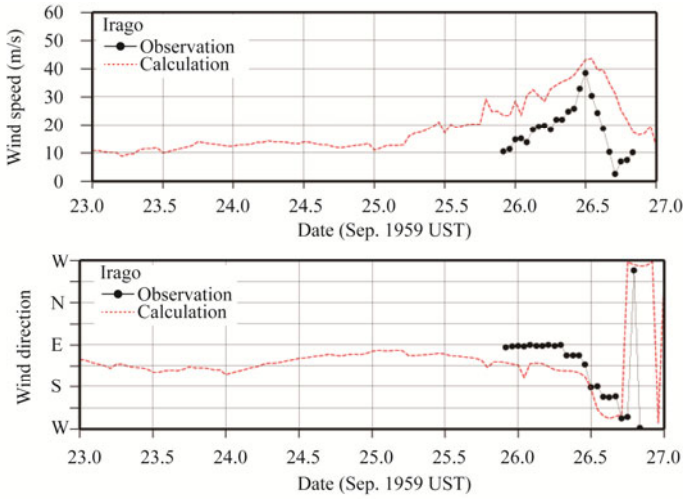

Fig. 7. (Continued) Comparison of observed and calculated wind data at Tsu, Isewan-sea-berth and Irago Stations.

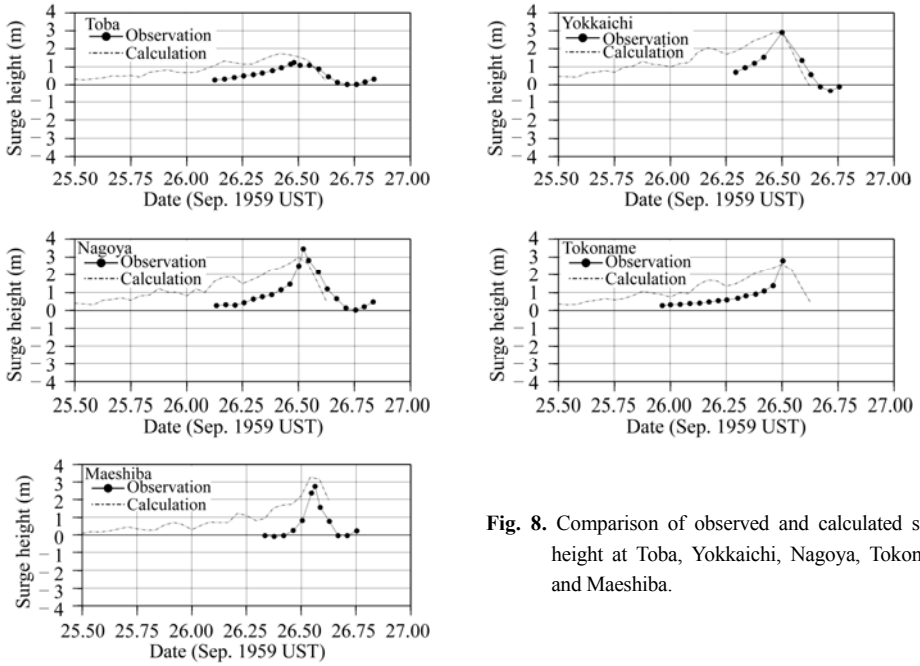

Fig. 8. Comparison of observed and calculated surge height at Toba, Yokkaichi, Nagoya, Tokoname and Maeshiba.

The wave data such as the significant wave height and wave period are calculated from the coupled tide-surge-wave model. A prior study that reported a comparison of the coupled tide-surge-wave model (ADCIRC-UnSWAN) and wave model (UnSWAN) showed that the significant wave height estimated by the wave model only tended to be somewhat larger than that of the coupled model (Kim *et al*., 2013b). Fig. 11 shows the locations of stations for wave observation along the southeast coast of Japan. The points shown in the bottom figure indicate the stations where our results are compared with the TTRI estimates. Table 1 shows the comparison of the observation and calculation of wave characteristics at four stations that are shown in Fig. 11. Regarding the sign of the wave height,

the difference between the observations and calculation is not significant except for the Shimizu Station. With regard to the time when the maximum significant wave appeared, the time was estimated to be later by 3−6 hours compared with the observation time, except for the Naarai Station. However, the calculated wave period generally agrees with the observation data. Unlike in the Ise Bay, the modeled area including four stations along the Pacific Coast is not covered with the high-resolution mesh. Therefore, the locations of the observations and calculation do not match each other. Despite some limitations like those described above, the model developed in this study seems to appropriately calculate the wave characteristics across most of the model domain.

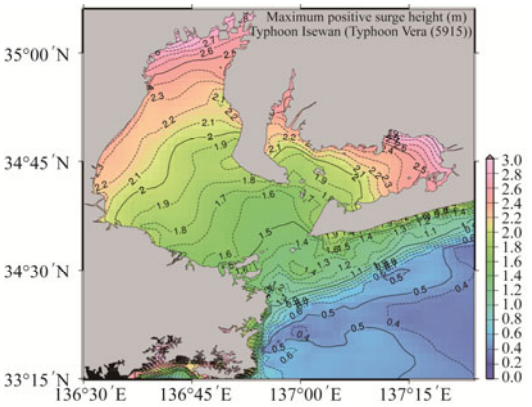

Fig. 9. Maximum positive surge height due to the typhoon Isewan.

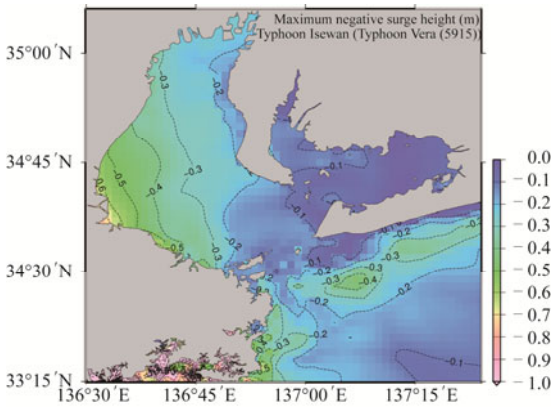

Fig. 10. Maximum negative surge height due to the typhoon Isewan.

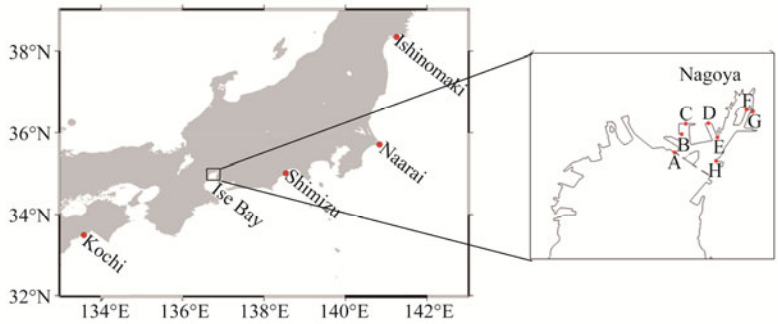

Fig. 11. Stations for the comparison of wave. Left panel: stations of wave observations, right panel: stations of TTRI's wave estimation (1959).

Table 1 Comparison of wave characteristics on the Pacific Coast

Stations	Max. significant wave height (m)		Wave period (s)		Time (JST) of appearance	
	Obs.	Cal.	Obs.	Cal.	Obs.	Cal.
Kochi	6.5	8.9	14.4	18.5	20:00 26th	17:00 26th
Shimizu	4.2	13.9	17.0	12.5	01:00 27th	21:00 26th
Naarai	2.9−3.0	2.4	10.5−13.0	11.5	08:00−14:00 26th	21:00 26th
Ishinomaki	4.0	7.1	11.0	10.4	06:00 27th	00:00 27th

Note: Obs.−wave observation data shown in TTRI's report (1959); Cal.− wave data calculated by this study.

The significant wave height of 2 m was found after the typhoon passed Nagoya (Fig. 12). The significant wave height was approximately 10 m at the entrance of the Ise Bay and rapidly decreased after entering the bay; it then become approximately 2 m in the northern end (near Nagoya City) of the bay. The maximum wave height simulated inside the bay is similar to that from previous studies (Shibaki *et al*., 1998, 2007; Yamaguchi *et al*., 2012). The decrease in wave heights observed inside the bay is caused by shoaling, blocking due to the topographic feature of the bay's mouth, and wave breaking (Shibaki *et al*., 2007).

The maximum mean period ranges from 4 to 7 s in the Ise Bay (Fig. 13). The significant wave period (T_s) is inferred from the relation $T_s \fallingdotseq 1.1-1.2\ T_m$ (mean wave period) (Goda, 1974, 2008). The significant wave period estimated from the wave model was reported at 4−6 s inside the Ise Bay and occured around the time when the typhoon Isewan was closest to the Ise Bay (Kobayashi, 2002). Therefore, the wave period can also be reasonably reproduced based on the coupled wave-tide-surge model in our study.

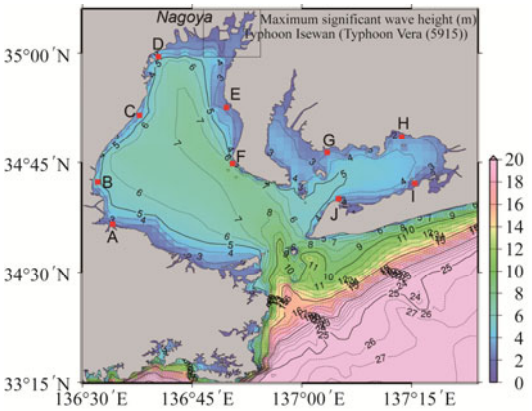

Fig. 12. Maximum significant wave height due to the typhoon Isewan. The uppermost rectangular area indicates the area shown in the right panel in Fig. 11.

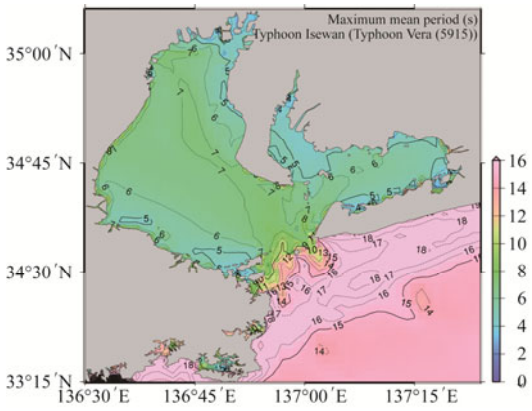

Fig. 13. Maximum mean period due to the typhoon Isewan.

The TTRI (1959) estimated the predominant wave height and wave direction by using information from the investigation of damages of the coastal structures, i.e., seawalls, breakwaters, and groins. Table 2 indicates the TTRI estimates near the major cities in the Ise Bay, which is used for a comparison with our results. In general, our estimated wave heights are somewhat larger than the TTRI results, except for Point I (near Tahara City) showing the largest difference of 1.6 m among all differences, but our estimation seems to be in the acceptable range. Our calculated wave directions are very close to the TTRI results.

From the results for the Ise Bay, this study shows that the maximum significant wave height varies from 1.7 to 3.6 m near the coast, and the largest value is found at Point D (near Yokkaichi City), which is the same as that in the TTRI report. The TTRI (1959) reported that the prevailing significant wave height was the maximum of approximately 4 m on the northwest coast and the minimum of approximately 2 m near the coast of the Nagoya Port. The report also stated that the wave height on the

east coast was approximately 80% of the height along the west coast. From Fig. 12 and Table 2, it is understood that the wave height from this study follows the trend of the TTRI wave height, and the ratio of the wave heights of the east to those of the west is 72%−79%, if we divide the average wave heights at points E−J or E−F along the east coast by the averages at points A−D along the west coast.

Table 2 Comparison of wave characteristics in the Ise Bay (points shown in Fig. 12)

Points	City	Direction		Max. significant wave height (m)	
		TTRI	Cal.	TTRI	Cal.
A	Matsuzaka	E	E	2.0	2.1
B	Tsu	E−ESE	ESE	3.0	3.0
C	Chiyozaki	SE−SSE	SE	2.5	3.0
D	Yokkaichi	SE−S	SE	3.3	3.6
E	Tokoname	SW−SSSW	SSW	2.0	1.9
F	Noma	SW−SSWS	SSW	2.0	2.7
G	Yoshida	-	SSE	1.5	2.1
H	Gamagori	-	SSE	1.5	1.7
I	Tahara	-	W	0.8	2.4
J	Fukue	-	ENE	1.5	1.8

Note: TTRI− wave data calculated by TTRI's method (TTRI, 1959); Cal.− wave data calculated by this study.

Because Nagoya City was very seriously attacked by the typhoon Isewan, we evaluated the wave characteristics in detail around Nagoya City. The right panel of Fig. 11 shows the location of points around Nagoya City. As shown in Table 3, TTRI (1959) results included wave direction, maximum significant wave height, wave period and time of appearance by using their graphical method. Our calculated wave directions are close in value to the TTRI results, and it is found that the prevailing wind direction in this area is SSE−WSW. Regarding the significant wave height, our calculation ranges from 0.8 to 3.4 m, and similar to the results for the Ise Bay, our wave heights are generally slightly larger than the TTRI results. However, the calculated wave periods are close to the TTRI results, and the wave period ranges from 2.9 to 6.2 s. Additionally, the time of appearance is compared, and a difference of at most 1.8 hours is obtained. The model outputs for the wave characteristics such as the significant wave height, wave period and direction were set to be recorded at an interval of 1 hour. Therefore, it is difficult to compare the time of appearance in minutes. From these results, it is found that the time when the maximum significant wave height occurs is approximately 22:00−23:00 on the 26th.

Table 3 Comparison of wave characteristics near Nagoya Port (points shown in Fig. 11)

Points	Direction		Max. Sig. wave height (m)		Wave period (s)		Time (JST) of appearance	
	TTRI	Cal.	TTRI	Cal.	TTRI	Cal.	TTRI	Cal.
A	S	S	2.20	3.37	5.8	6.2	22:08 26th	22:00 26th
B	S	SSE	1.90	1.85	5.4	3.7	21:59 26th	21:00 26th
C	SSSW	S	1.65	1.82	4.5	3.6	22:09 26th	21:00 26th
D	SSSW	SSE	1.65	1.81	4.6	3.6	22:06 26th	21:00 26th
E	SSW	SSW	2.05	2.40	5.3	4.2	23:22 26th	23:00 26th
F	SSW−SW	SSE	1.85	1.39	5.0	3.2	23:20 26th	21:00 26th
G	SW	WSW	1.50	0.80	4.5	2.9	00:45 27th	23:00 26th
H	SW−WSW	SW	1.40	2.23	5.1	4.1	00:23 27th	23:00 26th

Note: TTRI− wave data calculated by TTRI's method (TTRI, 1959); Cal.− wave data calculated by this study.

The storm surge and wave characteristics calculated based on our modeling are compared and

evaluated with the observations and results of previous studies. Despite the difference in estimation methods, our study shows a similar distribution to those shown in other studies and is within the acceptable range of variation.

5. Conclusions

The simulations of the typhoon Isewan by using the coupled model yield reasonable results when compared with observations and results of previous studies. The integrally coupled model developed in this study can reasonably simulate the storm surge and waves for extreme typhoon conditions in 1959 for the Ise Bay.

In the current study, the ADCIRC-UnSWAN system was found to be sufficiently appropriate for the hindcast simulation of coupled processes of wave-tide-surges in the deep open and shelf sea regions. This coupled system is a good starting point for operational wave-tide-surge forecasting and can be easily extended to regional sites of interest without significant increases in computational burden. There is, however, an obvious need for further refinement and extension of the system. The immediate concern is to introduce a diffraction term and higher-order propagation scheme into the spectral wind wave model, especially for applications to engineering problems. The developed system uses a set of depth-integrated equations so that the vertical structure of the currents, radiation stress, surface stress and bottom boundary layer are simplified. In the future, extension of the system to three dimensions will be required.

References

Atkinson, J. H., Westerink, J. J. and Hervouet, J. M., 2004. Similarities between the wave equation and the quasi-bubble solutions to the shallow water equations, *Int. J. Numer. Methods Fluids*, **45**(7): 689−714.

Booij, N., Ris, R. C. and Holthuijsen, L. H., 1999. A third-generation wave model for coastal regions, Part I, Model description and validation, *J. Geophys. Res.*, **104**(C4): 7649−7666.

Bunya, S., Dietrich, J. C., Westerink, J. J., Ebersole, B. A., Smith, J. M., Atkinson, J. H., Jensen, R., Resio, D. T., Luettich, R. A., Dawson, C., Cardone, V. J., Cox, A. T., Powell, M. D., Westerink, H. J. and Roberts, H. J., 2010. A high resolution coupled riverine flow, tide, wind, wind wave, and storm surge model for southern Louisiana and Mississippi, Part I: Model development and validation, *Mon. Weather Rev.*, **138**(2): 345−377.

Cardone, V. J., 1969. *Specification of the Wind Distribution in the Marine Boundary Layer for Wave Forecasting*, Tech. Rep. 69-1, Geophysical Sciences Laboratory, New York University, 131.

Central Disaster Management Council, 2003. *Report of the Technical Investigation Committee on Earthquakes in the Vicinity of the Japan Trench*, Cabinet Office, Government of Japan. (in Japanese)

Choi, B. H., Min, B. I., Kim K. O. and Yuk, J. H., 2013. Wave-tide-surge coupled simulation for typhoon Maemi, *China Ocean Eng.*, **27**(2): 141−158.

Dietrich, J. C., Bunya, S., Westerink, J. J., Ebersole, B. A., Smith, J. M., Atkinson, J. H., Jensen, R., Resio, D. T., Luettich, R. A., Dawson, C., Cardone, V. J., Cox, A. T., Powell, M. D., Westerink, H. J. and Roberts, H. J., 2010. A high resolution coupled riverine flow, tide, wind, wind wave and storm surge model for southern Louisiana and Mississippi: Part II − Synoptic description and analyses of Hurricanes Katrina and Rita, *Mon. Weather Rev.*, **138**(2): 378−404.

Goda, Y., 1974. Estimation of wave statistics from spectral information, *Proc. Int. Symp.* "*Ocean Wave Measurement and Analysis, waves'74*", ASCE, New Orleans, 320−337.

Goda, Y., 2008. Overview on the applications of random wave concept in coastal engineering, *Proc. Japan Acad., Ser. B*, **84**(9): 374−392.

Dawson, C., Westerink, J. J., Feyen, J. C. and Pothina, D., 2006. Continuous, discontinuous and coupled discontinuous-continuous Galerkin finite element methods for the shallow water equations, *Int. J. Numer. Methods Fluids*, **52**(1): 63−88.

Dietrich, J. C., Zijlema, M., Westerink, J. J., Holthuijsen, L. H., Dawson, C., Luettich Jr. R. A., Jensen, R. E., Smith, J. M., Stelling, G. S. and Stone, G. W., 2011. Modeling hurricane waves and storm surge using integrally-coupled, scalable computations, *Coast. Eng.*, **58**(1): 45−65.

Fujita, T., 1952. Pressure distribution within typhoon, *Geophysics Magazine*, **23**(4): 437−451.

Holthuijsen, L. H., Herman, A. and Booij, N., 2003. Phase-decoupled refraction-diffraction for spectral wave models, *Coast. Eng.*, **49**(4)**:** 291−305.

JMA (Japan Meteorological Agency), 1961. *Report of the Ise Bay Typhoon* (*No. 5915*) *in September 1959*, Technical Report of the Japan Meteorological Agency No. 7, 467.

Jones, M. T., 2003. *GEBCO Digital Atlas*: *Centenary Edition of the IHO/IOC General Bathymetric Chart of the Oceans* [CD-ROM], Natl. Environ. Res. Counc., Swindon, U. K.

JWF (Japan Water Forum), 2005. *Typhoon Isewan (Vera) and Its Lesson*, 60.

Kawasaki, K., Niwa, T. and Mizutani, N., 2010. Development of storm surge and high wave-induced inundation model considering influence of high wave and its accuracy validation, *Japan Society of Civil Engineers*, *Ser. B2* (*Coastal Engineering*), **66**(1): 196−200. (in Japanese with English Abstract)

Kim, K. O., Choi, B. H. and Yuk, J. H., 2013a. Wave hindcast from integrally coupled wave-tide-surge model of the East China Sea, *Proc. 7th International Conference on Asian Pacific Coast* (*APAC2013*), 714−721.

Kim, K. O., Yuk, J. H., Jung, K. T. and Choi, B. H., 2013b. Simulation of typhoon Bolaven using integrally coupled tide-surge-wave models based on unstructured grid system, *Proc. Korean Associated of Ocean Science and Technology Societies*, 1646−1649.

Kobayashi, T., 2002. *Sea Wave Model and Its Application*, The Series 02-B-7 in Water Engineering of Japan Society of Civil Engineers, 1−20. (in Japanese)

Luettich, R. A. and Westerink, J. J., 2004. *Formulation and Numerical Implementation of the 2D/3D ADCIRC Finite Element Model*, version 44.XX, http://adcirc.org/adcirc_theory_2004_12_08.pdf.

Matsumoto, K., Takanezawa, T. and Ooe, M., 2000. Ocean tide models developed by assimilating TOPEX/POSEIDON altimeter data into hydrodynamical model: A global model and a regional model around Japan, *J. Oceanogr.*, **56**, 567−581.

Shibaki, H., Aono, T., Mikami, T. and Goto, C., 1998. Development of integrated numerical research system for prevention and estimation of coastal disaster, *Journal of Japan Society of Civil Engineers*, **II-42**, 77−92. (in Japanese with English Abstract)

Shibaki, H., 2004. *A study on Numerical Simulation of Wave-Surge-Tsunami and Application of Coastal Disaster Prevention Support System*, Ph. D. Thesis. (in Japanese)

Shibaki, H., Suzuyama, K., Kim, J. I. and Sun, L., 2007. Numerical simulation of storm surge inundation induced by overflow, overtopping and dike breach, *Proc. 4th International Conference Asian and Pacific Coasts* (*APAC2007*), 388−401.

TTRI (Transportation Technical Research Institute), 1959. *Storm, Surge and Damages Caused by Typhoon No. 15*, 44.

Westerink, J. J., Luettich, R. A., Feyen, J. C., Atkinson, J. H., Dawson, C., Roberts, H. J., Powell, M. D., Dunion, J. P., Kubatko, E. J. and Pourtaheri, H., 2008. A basin to channel scale unstructured grid hurricane storm surge model applied to southern Louisiana, *Mon. Weather Rev.*, **136**(3): 833−864.

Yamaguchi, M., Ohfuku, M., Nonaka, H., Hino, M. and Hatada, Y., 2010. Wind distributions on the inland sea and inner bays of Japan generated by the 3 monster typhoons in the Showa Era, *Annual Journal of Hydraulics Engineering*, **54**, 1567−1572. (in Japanese with English Abstract)

Yamaguchi, M., Hatada, Y., Ohfuku, M. and Nonaka, H., 2012. Estimating extremes of wind speeds and wave heights generated by intense storms during the 1921-2005 year period in Ise Bay, *Annual Journal of Engineering Ehime University*, **11**, 70−92. (in Japanese with English Abstract)

Yamaguchi, M., Hatada, Y., Ohfuku, M. and Nonaka, H., 2013a. Figure collections for space-time variations of sea surface winds and wave heights induced by abnormally strong typhoons during the period of 1917-1972 in the Seto Inland Sea, Ise Bay and Tokyo Bay, *Annual Journal of Engineering Ehime University*, **12**, 46−85. (in Japanese with English Abstract)

Yamaguchi, M., Ohfuku, M., Nonaka, H. and Hatada, Y., 2013b. Figure collections for spatial distributions of the lowest sea level pressure induced by strong typhoons during the period of 1911-1972 on the Seto Inland Sea, Ise Bay and Kanto Sea Area, *Annual Journal of Engineering Ehime University*, **12**, 86−102. (in Japanese with English Abstract)

Zijlema, M., 2010. Computation of wind-wave spectra in coastal waters with SWAN on unstructured grids, *Coast. Eng.*, **57**, 267−277.